Tellus (1982), 34, 409–428

Evaluation of lateral boundary errors in a limited-domain model

By DAVID P. BAUMHEFNER and DONALD J. PERKEY[1], *National Center for Atmospheric Research[2], Boulder, Colorado 80307, USA*

(Manuscript received July 14, 1981; in final form January 14, 1982)

ABSTRACT

Computational errors that arise from the imposition of artificial lateral boundaries in numerical forecast models are evaluated, using the Perkey–Kreitzberg method of variable tendency averaging near the boundary in the NCAR second generation Limited Area Model. Boundary error is diagnosed for two sets of initial conditions by using an unbounded forecast as background truth. Several components of boundary error are identified and evaluated. These include the accuracy of the boundary specification, the formulation of the blending, the increased boundary diffusion, and the physical location of the boundary. The formulation is tested by comparing boundary errors generated by the Williamson–Browning method for the same initial conditions. Finally, the boundary errors are compared to the total forecast error to evaluate its significance.

Results indicate the Perkey–Kreitzberg method is stable for a wide variety of resolutions and situations. Significant errors propagate inward from the boundaries at speeds of 20–30° longitude per day. Inaccuracies in the data specified at the boundary can account for a major part of these errors, while increased diffusion near the boundary plays a lesser role in error generation. The two formulations produce similar error structures, but with less generation of spurious transients in the Williamson–Browning method. However this method proved to be unstable at high horizontal resolutions. In general, the boundary error is much less than the total forecast error.

1. Introduction

There is increasing evidence that many weather-producing events are associated with atmospheric scales too small to be accurately resolved by grid-mesh sizes now feasible in global numerical models. Therefore a need for very-fine mesh numerical models has developed which for practical purposes must be limited in domain extent. In fact models of this type are currently being used operationally in many national weather services as well as for general research. The imposition of lateral boundaries in numerical models produces additional forecast error which would not be present in an unbounded forecast. It is important to evaluate the nature of these errors and their relationship to the total forecast error. Knowledge of the lateral boundary error will establish the relative accuracy of model forecasts made from limited domains and will give the user a sense of confidence regarding the model products.

Because the atmosphere contains large and small scales that sometimes rapidly interact with each other, the weather phenomena being modeled within a limited domain should be allowed to interact with large-scale atmospheric states that evolve at the model's artificial boundaries. Two basic strategies have been suggested to provide the finer-mesh model with information from outside its domain; (1) embed the finer-mesh domain within a coarser-mesh region, both of which are integrated simultaneously, thus providing for informational flow from the coarse mesh to the fine mesh and vice versa, or (2) embed the finer-mesh domain within a

[1] Present affiliation: Dept. of Physics & Atmos. Science, Drexel University, Philadelphia, PA 19104, U.S.A.

[2] The National Center for Atmospheric Research is sponsored by the National Science Foundation.

0040-2826/82/050409-20$02.50/0

coarser-mesh region which has been previously integrated, thus allowing the fine mesh to only react to information from the coarse mesh.

Examples of the first method, referred to as a two-way interacting system, are described in Harrison and Elsberry (1972), Phillips and Shukla (1973), Phillips (1978), and Staniforth and Mitchell (1978). Phillips' technique uses a hemispheric grid point model with discrete changes in resolution to a fine mesh. Staniforth and Mitchell constructed a finite element model which allows a smoothly varying grid structure. Examples of the second method were developed by Charney et al. (1950), Shapiro and O'Brien (1970), Asselin (1972), Kesel and Winninghoff (1972), and Anthes (1974). These papers represent a wide variety of approaches to the problem of one-way reactive boundary conditions. Differences in the two basic strategies are substantial from a technical point of view. This fact discourages meaningful comparisons between these techniques and we therefore will not address this problem.

We will instead concentrate on the second of these strategies; one-way informational flow or parasitic nesting. To accomplish the requirements of this strategy, it is necessary to develop lateral boundary conditions which allow meteorological information from the coarse grid to both enter and exit from the fine mesh, and also allow information such as gravity waves which are created within the fine mesh to exit from the domain freely. Oliger and Sundström (1976) have shown for one-way reacting systems and for the multi-level baroclinic case, that the primitive hydrostatic meteorological equations are mathematically ill-posed with any specification of local, pointwise boundary conditions. In spite of this problem, several methods have been proposed; for example, Williamson and Browning (1974), Davies (1976), and Perkey and Kreitzberg (1976), which have been shown to be useful in limited domain forecasting. These schemes fall into two categories: (1) those which are based on an advection-type extrapolation, and (2) those which are based purely on a pragmatic or engineering approach. The first of these approaches argues that at inflow boundaries (those at which the normal component of the wind is into the domain), the boundary conditions are predominantly determined by the coarse-grid state while at outflow boundaries (those with the normal component of wind out of the domain), the boundary conditions are predominantly determined by the fine-mesh state. These schemes can be traced to Charney et al. (1950) who determined that specification of both the height and vorticity everywhere on the boundary leads to development of instabilities at the outflow boundary which propagate back into the forecast domain.

The second approach, the pragmatic approach, is characterized by specification of all variables on all boundaries. The results of this overspecification are then controlled by increased damping or filtering in the boundary region. A large number of modelers have made use of this approach with a high degree of success in both research and operational models (Gerrity, 1977; Gauntlett et al., 1978; McGregor et al., 1978; Kållberg and Gibson, 1977; Hodur and Burk, 1978).

We will focus on evaluation of one example of the second approach, namely the Perkey–Kreitzberg method (Perkey and Kreitzberg, 1976; referred to as PK), using real atmospheric initial conditions and the baroclinic primitive equations. Perkey (1976) used the scheme for predictive purposes, but did not discuss the possible influence of the lateral boundary conditions on the results. The results of the evaluation of the PK system will then be compared to an example of the first approach, the Williamson–Browning method (Williamson and Browning, 1974; referred to as WB).

The purpose of this paper is to investigate the applicability of the PK method to the NCAR second generation Limited Area Model (LAM) for a variety of situations and evaluate the resulting error distributions that arise from such an application. An attempt is made to isolate and identify the various sources of error that result from integrations of laterally bounded forecast equations. Boundary errors are separated into two components: namely, those which are generated by the boundary formulations and those which result from the data specification at the boundary being inaccurate. A comparison is made with another method (WB) to see if the conclusions reached for the PK method can be generalized. The resulting lateral boundary errors for both systems are contrasted with the total error produced by the numerical prediction system in order to assess their relative impact on the forecast.

Section 2 briefly reviews the PK method while Section 3 describes the case studies used in the investigation. Section 4 discusses the boundary error generation from the PK method and Section 5 diagnoses the sources of these errors. Section 6 discusses the generality of the previous results by comparing PK and WB methods. The final section deals with the relationship of the boundary error to the forecasted error.

2. Description of the Perkey–Kreitzberg scheme

A detailed description of the PK boundary conditions can be found in the original paper (Perkey and Kreitzberg, 1976); we briefly outline the basic structure of the method here. The PK scheme consists of linearly combining specified time-dependent tendencies with model calculated tendencies at the boundaries and the first three grid points inside the boundaries. That is, for any dependent variable χ

$$\left.\frac{\partial \chi}{\partial t}\right|_I = W(I)\left.\frac{\partial \chi_{\mathrm{m}}}{\partial t}\right|_I + [1 - W(I)]\left.\frac{\partial \chi_{\mathrm{ls}}}{\partial t}\right|_I, \quad (1)$$

where χ_{ls} denotes the specified (large-scale) tendency of χ and χ_{m}, the model calculated tendency of χ. The weighting coefficients W are as follows:

$$W(I) = \begin{cases} 0.0 \text{ for } I = \text{boundary grid points,} \\ 0.4 \text{ for } I = \text{boundary-1 grid points,} \\ 0.7 \text{ for } I = \text{boundary-2 grid points,} \\ 0.9 \text{ for } I = \text{boundary-3 grid points,} \\ 1.0 \text{ for } I = \text{all other interior grid points.} \end{cases} \quad (2)$$

Therefore, the tendency at the boundary is totally specified by the exterior value, while at the fourth grid point in the interior, the tendency is solely determined by the model. At grid points in between, the tendency is a blend of the specified and model calculated values. To complete this boundary system, increased diffusion or smoothing is also necessary around the boundary. The specified values along the boundaries of the limited domain are usually derived from a hemispheric model forecast using a coarser mesh. However, the boundary values may be specified in any manner chosen by the user. The PK system of linking the large-scale solution to the interior fine-scale solution is similar to other methods being used operationally and has been classified as a sponge damping technique (Sundström and Elvius, 1979). These techniques have been employed by the U.S. Navy's Fleet Numerical Weather Center (Kesel and Winninghoff, 1972) and the U.S. National Meteorological Center (Gerrity, 1977; Newell and Deaven, 1981) and have proven to be acceptable in the operational environment. Although we do not test the other methods in the sponge-damping category, we assume the errors produced by the PK system are somewhat representative of the group as a whole (Miyakoda and Rosati, 1977).

Application of the PK method to the LAM is fairly straightforward. Eqs. (1) and (2) were used to operate on the boundary region tendencies of all LAM prognostic variables, i.e., momentum, pressure, and density weighted specific humidity. The diffusion coefficient used in the deformation-type scheme (Washington and Kasahara, 1970) is systematically increased to five times the normal value as the boundary is approached. However, because the PK system is applied to the tendencies, the resulting smoothing is less than might be expected. To demonstrate this difference, we write the tendency equation for a simple one-dimensional diffusion model:

$$\frac{\partial \chi_{\mathrm{m}}(x)}{\partial t} = K(x)\frac{\partial^2 \chi(x)}{\partial x^2}. \quad (3)$$

Next we apply eqs. (1) and (2) which yields

$$\frac{\partial \chi(x)}{\partial t} = W(x)\,K(x)\frac{\partial^2 \chi(x)}{\partial x^2} + [1 - W(x)]\frac{\partial \chi_{\mathrm{ls}}(x)}{\partial t} \quad (4)$$

Note that because of the weighting term, the diffusion coefficient (K) is effectively reduced at the boundaries when applied in the above manner. This counteracts the effects of increasing K around the boundaries. As is demonstrated by one of the experiments discussed in Section 5, this can be overcome by including the diffusion part of the tendency after the boundary modification has been applied. This results in a more effective increase in diffusion.

3. Methodology and verification strategy

In order to separate the forecast error produced by the boundary conditions from the total error

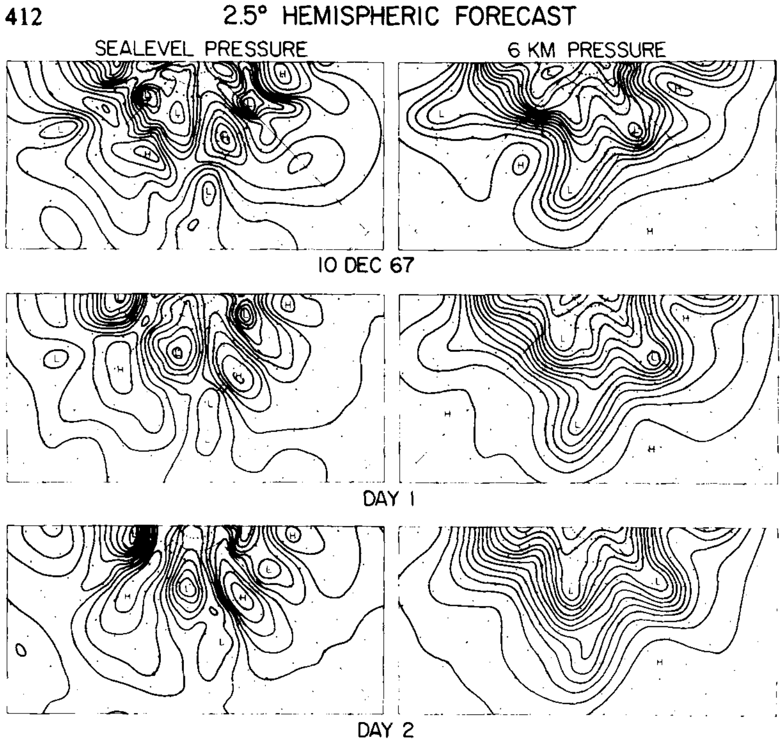

Fig. 1. Initial state (top), 24 h forecast (middle), and 48 h forecast (bottom) of the sea level pressure (left) and the 6 km pressure (right) derived from a 2.5° latitude/longitude, hemispheric model. Initial data for December 10, 1967, 1200 GMT. Contour interval equals 4 mb. Area outlined indicates limited domain of integration.

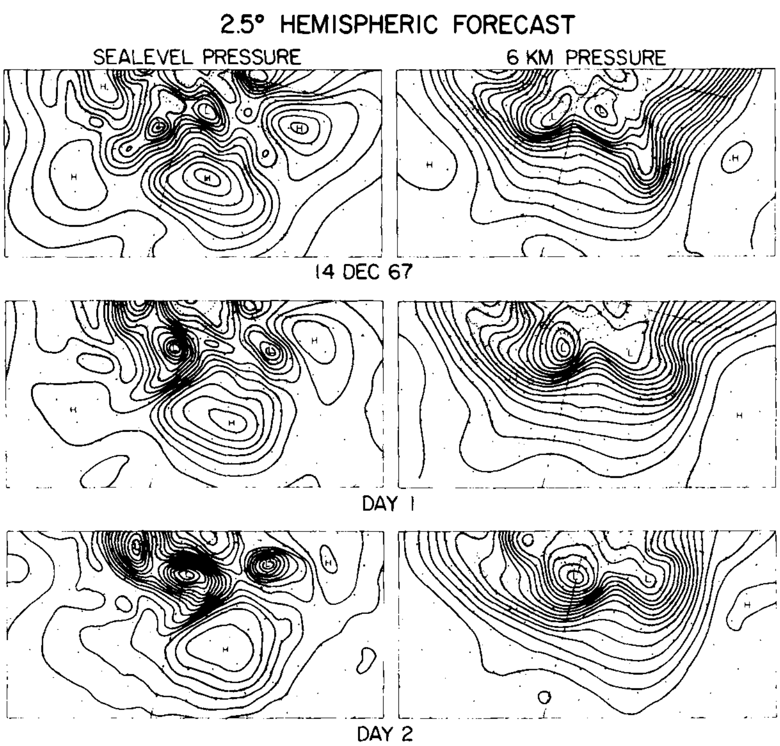

field, we use an unbounded hemispheric model forecast as our basis of verification. If the hemispheric and limited domain model's configurations are kept identical, except for the lateral boundaries, then a difference field between the two forecasts reveals the boundary condition errors. This, of course, does not represent the actual error of the model with respect to the atmosphere. We compare the boundary error with the total forecast error in a later section.

Two cases were selected to test the boundary conditions. Together they represent a typical sample of the various types of mid-latitude systems that may enter or exit from the domain and influence the resulting forecast. The initial conditions and the 2.5° hemispheric model (Washington et al., 1977) forecasts for 24 and 48 h which will be used as though they represent "truth" for verification purposes are displayed in Figs. 1–2. The initial geopotential data for these forecasts were subjectively analyzed (Baumhefner et al., 1978) and a filtered geostrophic wind was calculated to initialize the velocity field (Washington and Baumhefner, 1975).

The 1200 GMT December 10, 1967 case, Fig. 1, shows a progression of three transient systems over the limited domain (outlined by the solid longitude/latitude line). The trough on the western boundary enters the domain during the forecast and amplifies considerably. A large ridge replaces the western trough at the boundary both at the surface and in the middle troposphere. A trough, originally along the east coast, moves eastward through the boundary during the forecast. The system over the central U.S. translates slowly eastward and decays slightly, but does not approach a boundary.

The second case, 1200 GMT December 14, 1967 (Fig. 2) which is centered over E. Asia, displays less activity in the southern latitudes with a large arctic high dominating the pattern. However, the northern storm track is more active with very strong systems entering and leaving the domain. A rapidly developing baroclinic wave along the western boundary changes the flow field dramatically and a strong jet streak enters the boundary associated with this development. A major cyclonic development occurs within the domain and propagates toward the NE corner replacing a ridge at the boundary. The following discussion of boundary error will stress the interaction of these various synoptic features with the evolving error fields.

4. Boundary error generation

The model configuration used to determine the lateral boundary condition errors was designed to simulate an operational environment where the specified boundary information is produced by a coarse-mesh model. Thus, errors due to the inaccuracy of the specification and to the formulation of the boundary condition contribute to the boundary error. To isolate the formulation error, a boundary specification with the same resolution as the interior was tested and will be discussed in Section 5.

The limited domain model (Valent et al., 1977) consisted of a 2.5° latitude/longitude grid over a 90° longitude by 75° latitude window. It had six evenly spaced layers in the vertical with the top at 18 km. The boundary information was provided at each time step by a 5° latitude/longitude model that was global in domain (Washington and Kasahara, 1970). Both models used the same vertical configuration and physical parameterizations, and for simplicity did not include a mountainous lower boundary. Later experiments with mountains added to the limited domain model did not appreciably change the results reported here.

The initial data (refer to section 3) for both models were derived from a gridded geopotential analysis on a 2.5° mesh. The geostrophic wind was calculated and filtered on this mesh. The 5° global model which produced the boundary information was initialized by using every other grid point from the 2.5° data. In order to more clearly see the effects of the boundary error on the larger scales, the forecast output from all models shown here was filtered to remove all of the amplitude of the smallest-scale components generated by the model.

The time evolution of the boundary error produced by the PK formulation is shown in Fig. 3

Fig. 2. Initial state (top), 24 h forecast (middle), and 48 h forecast (bottom) of the sea level pressure (left) and the 6 km pressure (right) derived from a 2.5° latitude/longitude, hemispheric model. Initial data for December 14, 1967, 1200 GMT, centered over E. Asia. Contour interval equals 4 mb. Area outlined indicates limited domain of integration.

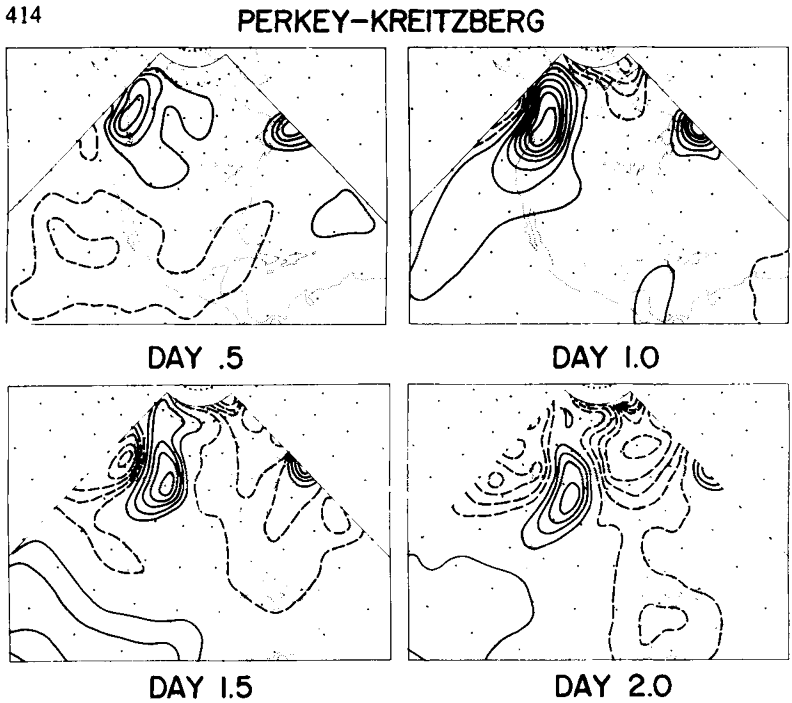

Fig. 3. Difference between bounded and unbounded 6 km pressure forecasts at 12 h (top left); 24 h (top right); 36 h (bottom left); 48 h (bottom right) using December 10, 1967, 1200 GMT initial conditions and the Perkey–Kreitzberg boundary condition. Contour interval = 1 mb. Negative values are dashed.

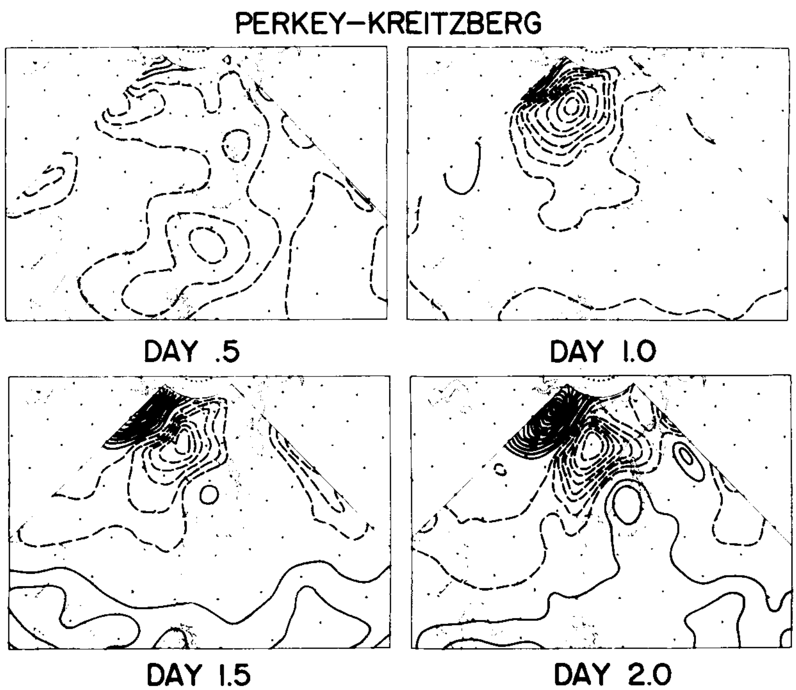

Fig. 4. Difference between bounded and unbounded 6 km pressure forecasts at 12 h (top left); 24 h (top right); 36 h (bottom left); 48 h (bottom right) using December 14, 1967, 1200 GMT initial conditions and the Perkey–Kreitzberg boundary condition. Contour interval = 1 mb. Negative values are dashed.

for the first case, December 10, 1967. The errors are illustrated for pressure at 6 km (approximately 500 mb) and are representative of other levels not shown. The PK method produces a large error early in the forecast period with values reaching 7 mb (~100 m) at 24 h near the western boundary. A 1–2 mb error which develops in the subtropical areas is noticeable at 12 h, but appears to damp out with time. Large errors are generated where significant changes are taking place at the boundaries (refer to Fig. 1). These errors appear to have time continuity and propagate inward at a rate of 20–30° of longitude per day. For example, the positive error over British Columbia at 12 h advances to the Northern Rockies in 36 h. A major component of these errors is related to a loss of amplitude in synoptic features as they enter the domain. Positive errors are correlated with troughs and negative values with ridges indicating a smoothing of waves in the bounded forecast.

A paper by Miyakoda and Rosati (1977) discussed a similar propagation of error for four other boundary condition treatments. For our particular choice of domain the central area of the U.S. remains uncontaminated by boundary error until 36 h into the forecast. However, by 48 h the entire domain is filled with significant boundary error. The rate of error growth appears to be stabilizing during the latter part of the forecast.

The second case was tested to determine the sensitivity of previous results to different initial conditions. The boundary errors generated from the initial conditions on December 14, 1967 (see Fig. 2) are displayed in Fig. 4, for each 12 h period.

Many of the features noted in the first case can also be found in the second case. The propagation of error inward from active regions on the boundary is present; however, the error growth and propagation speed are somewhat faster. The loss in amplitude of features entering the domain is again noted. Rapid error growths early in the forecast period tend to stabilize after 36 h, but the entire domain still becomes contaminated with sizeable boundary error at 48 h. The initial oscillation found in the previous case is also present here and decreases in amplitude with time. The magnitude of error is considerably higher in this case, in the NW corner, perhaps related to the strong synoptic activity in the region.

Other tests were made with the PK boundary conditions in which the computational resolution was increased horizontally to a .625° grid and vertically to 24 layers. The 5° global model again provided the boundary specification. This configuration allowed a check on the stability of the scheme when large differences exist between the interior grid and the boundary grid. An evaluation of the high resolution boundary error was not made, because a hemispheric verification forecast was not available.

In order to more objectively illustrate results obtained from the subjective examination of the error distribution maps, the RMS, standard deviation, mean and S1 (Teweles and Wobus,

Table 1. *500 mb geopotential root mean square error (RMS), standard deviation, mean and S1 scores of the error field for the total area of the grid and a subset area (points within 20% of boundary excluded). Errors derived from PK scheme. RMS, std dev., and mean values in meters. S1 values are non-dimensional*

	Total area (subset area)			
Time	RMS	Std dev.	Mean	S1
December 10, 1967, 1200 GMT				
12H	18.9 (15.9)	18.8 (15.2)	−1.2 (−2.8)	21.1 (10.8)
24H	28.7 (26.5)	27.6 (22.7)	8.1 (13.7)	26.4 (11.9)
36H	27.0 (26.1)	26.9 (25.5)	−2.3 (−5.6)	27.4 (14.8)
48H	31.7 (29.7)	30.0 (29.3)	−10.0 (−5.1)	26.9 (18.7)
December 14, 1967, 1200 GMT				
12H	20.6 (22.9)	15.0 (12.6)	−14.1 (−19.1)	18.0 (8.1)
24H	29.4 (25.4)	25.7 (20.2)	−14.3 (−15.4)	23.4 (10.1)
36H	35.1 (23.0)	35.0 (19.1)	2.0 (−12.9)	27.6 (12.5)
48H	44.3 (34.2)	44.1 (32.8)	4.0 (−9.5)	33.1 (21.2)

1954) error values were calculated from all the grid points for the total limited domain and a subset of the domain. The subset values exclude all points within 20° latitude/longitude from the boundary. These error statistics are listed in Table 1 for both sets of initial conditions.

The statistics reveal many of the points mentioned in the previous discussion. A rapid error growth is apparent in the early phases of the forecasts followed by a leveling off or stabilizing effect. This behaviour is related to the excitation of spurious transients by the boundary conditions early in the forecasts which are subsequently damped as the forecast progresses. Such excitation or shocking during the integration produces a spectrum of waves, which are only partially removed by the increased diffusion near the boundary. Fortunately these transients probably do not interact with the slower moving meteorologically significant modes (Williamson, 1976). The statistical values of error are slightly less in the subset region which gives further evidence of the propagation of error from the boundary. This is somewhat obscured by the spurious excitation or shocking in the early periods. A comparison of these statistics with those produced by the Williamson–Browning boundary scheme is discussed in Section 6.

5. Boundary error sources

5.1. *Boundary specification*

The error generation of the PK lateral boundary conditions, while not dominating the interior, was quite significant near the boundaries. Further investigations were conducted to isolate and identify likely error sources. As mentioned before, the errors generated by boundary condition schemes may be subdivided into two categories: the specification error due to inaccurate values assigned at the boundary during the forecast and the formulation error which results from the blending of the assigned boundary values into the interior grid. We have attempted to ascertain the relative magnitudes of each of these error sources for the PK scheme. This can be accomplished by specifying the same resolution, or "perfect" boundary values, for the interior domain and comparing the resulting errors with 5° specification errors. Remember that the 2.5° boundary values are also used as the "truth" for error calculations.

The error distribution, using the "perfect" boundary specification, is shown at the bottom of Figs. 5–6 for the December 10, 1967 case. For comparison, the 5° boundary errors are repeated from Fig. 3 and the difference between the two unbounded forecasts at different resolutions is displayed at the top. In theory, the formulation error for the 2.5° boundary condition should reduce to zero, but in practice this is not the case. Even though the exact specification is given, the increased boundary diffusion is still operating and the boundary data is being interpolated to the model's staggered grid in space and time.

A substantial reduction in the amplitude of the errors occurred throughout the forecast except at 24 h. The shape and location of the error patterns remained remarkably similar. The error amplitude reduction approaches 50% in most cases. The 2.5° boundary error growth stabilizes in a manner similar to the 5° case reaching values of 2–3 mb (30–45 m) at 48 h.

The differences caused by resolution changes (Figs. 5–6, top) in unbounded forecasts show strong similarities to boundary error patterns in the limited domain after the first 12 h of the forecast. The magnitude of the boundary errors for the 5° specification are roughly twice the values produced by resolution differences. The 2.5° specification boundary error values are of similar magnitude.

Error statistics, shown in Fig. 7, were derived from these three comparisons in the manner of Staniforth and Mitchell (1978) to quantify the reduction in boundary error resulting from more accurate specification. These statistics also measure the net change in forecast accuracy of this limited domain model compared to an unbounded model at reduced resolution. The RMS and S1 scores were calculated from the differences shown in Figs. 5–6 for the total limited domain, a 20° and a 30° subset. A subset excludes the values nearest the boundary by the designated amount.

Comparing the dashed and dotted curves in Fig. 7 (top) to the difference fields reveals several interesting properties. It appears that the amount of error reduction produced by the exact 2.5° specification, as shown by the scores, is less than might be expected. However, the error variance (not shown) has, in fact, been reduced by a factor of 2 at 36 and 48 h in the total domain. The subset statistics do not show a clear-cut reduction in boundary error except at the latter stages of the

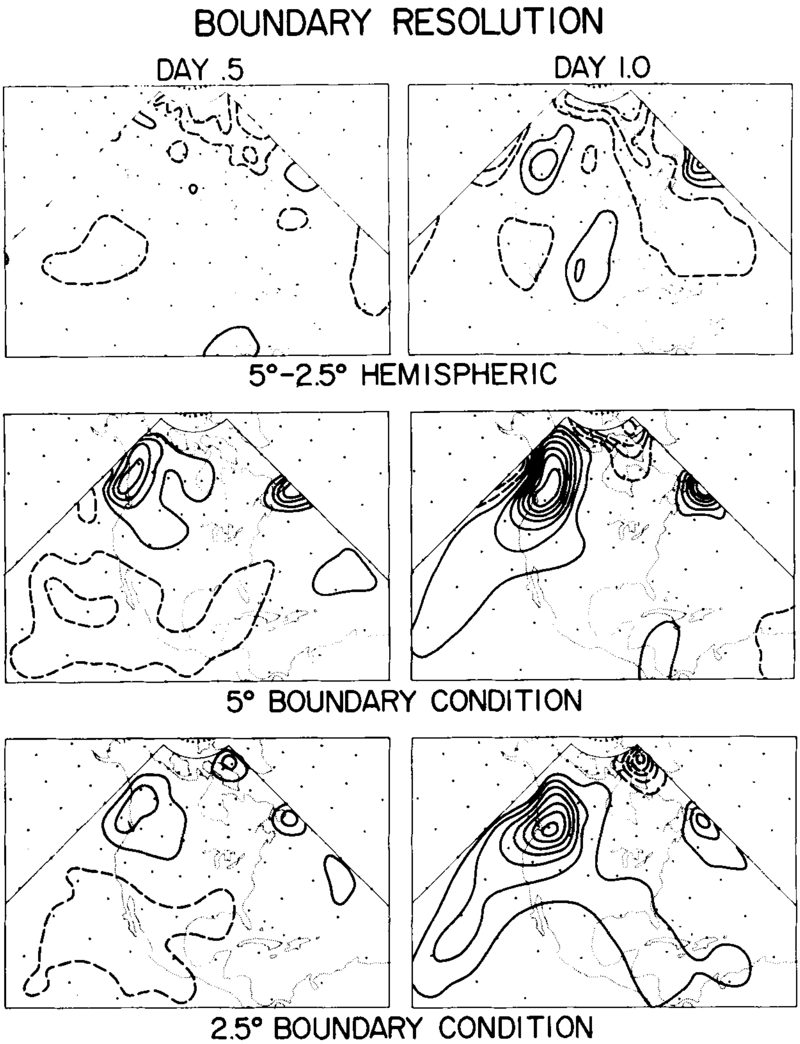

Fig. 5. Differences between unbounded 6 km pressure forecasts using 5° and 2.5° latitude/longitude horizontal grids (top). Differences between bounded and unbounded forecast using 5° model (middle) and 2.5° model (bottom) to specify boundary values. 12 h forecast (left) and 24 h forecast (right) shown. Contour interval = 1 mb with negative values dashed. Initial conditions from December 10, 1967, 1200 GMT.

forecast. The statistics for both boundary specifications illustrate a rapid growth of error of nearly the same magnitude early in the forecast and a more stable behavior thereafter. This characteristic is most likely caused by the previously discussed shocking phenomena generated by the boundary formulation. The inability of the formulation to remove this shocking is apparently masking some of the effect of the exact specification on the boundary early in the forecast. Since the S1 statistic is based on gradient and not absolute value, and is therefore less sensitive to large-scale transients, it shows a smoother error growth rate especially for the subsets. The reduction in error early in the forecast is more apparent in the S1 values.

If the boundary error statistics for both specifications are compared to the errors resulting from an unbounded coarse-mesh model (solid curve, Fig. 7), we find crossovers occurring from 24 to 48 h

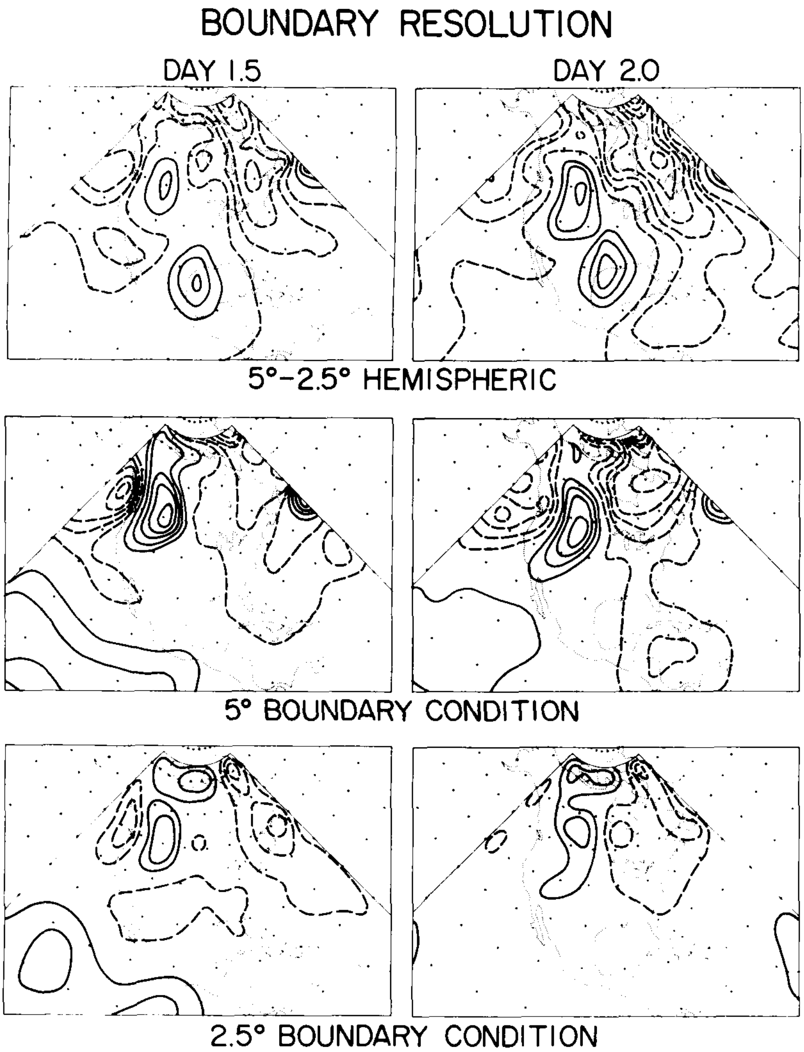

Fig. 6. Differences between unbounded 6 km pressure forecasts using 5° and 2.5° latitude/longitude horizontal grids (top). Differences between bounded and unbounded forecast using 5° model (middle) and 2.5° model (bottom) to specify boundary values. 36 h forecast (left) and 48 h forecast (right) shown. Contour interval = 1 mb with negative values dashed. Initial conditions from December 10, 1967, 1200 GMT.

into the forecast. Surprisingly, the 20 and 30° subset RMS statistics do not show any more skill than the total statistic. In a strict sense, this implies that forecasts made by the unbounded coarse-mesh model are more accurate than the limited-domain fine-mesh model early in the forecast. However, from examination of the time continuity of the actual differences, a large portion of the error early in the forecasts is due to excitation of rapidly moving spurious waves. The S1 values show less reaction to these waves with crossovers occurring in the subset statistics after only 12 h.

The comparison of coarse-mesh to limited domain skill was checked for another case, that of December 14, shown on the lower half of Fig. 7. For the total domain, the coarse-mesh is superior throughout the forecast. However, the subset statistics for RMS exhibited earlier crossover points than the December 10 case. The S1 subset values remained below the coarse-mesh values from the

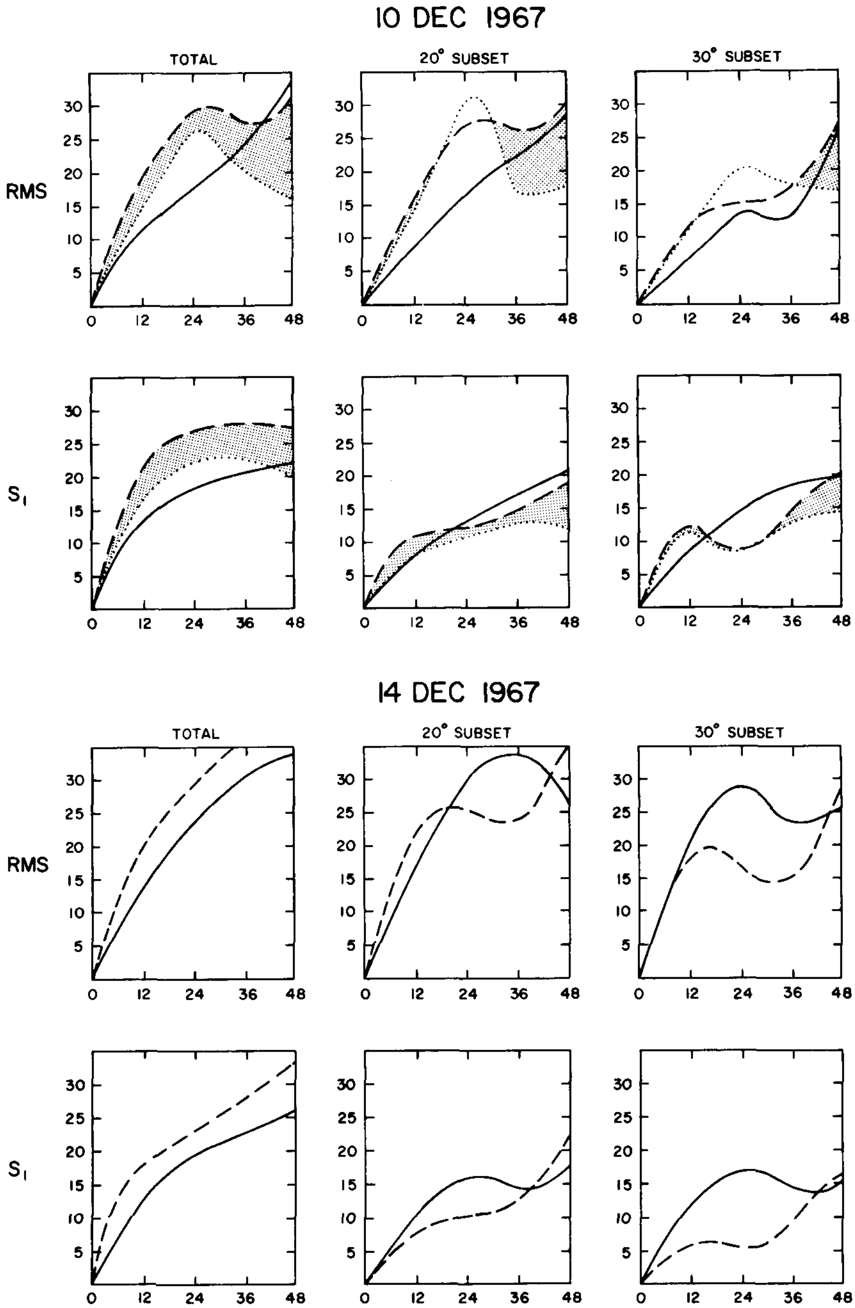

Fig. 7. RMS and S1 error statistics for two sets of initial conditions. December 10, 1967 case shown on top two rows; December 14, 1967 case on bottom two rows. Statistics calculated for total domain (left), 20° subset (middle), and 30° subset (right). Ordinate of all graphs represents (m) for RMS (top and middle bottom); abscissa represents hours of forecast. Solid line is difference error for 5° and 2.5° unbounded forecast. Dashed line is error from 2.5° limited domain forecast with specified 5° forecast boundaries. Dotted line is error from 2.5° bounded case with 2.5° forecast boundaries.

beginning. These results are more in line with the Staniforth and Mitchell (1978) calculations, but this implies a data dependency to this type of skill measurement. The forecast response of the synoptic situation to more accurate grid representation will exert some control over these statistical comparisons.

These results point to boundary specifications as being a major source of lateral boundary error. Research by Miyakoda and Rosati (1977) has shown similar results for all the methods they tested. They observe nearly the same reduction in error, the order of 50%, when a "perfect" boundary condition is used compared to a coarser mesh specification. Hovermale et al. (1977) and others have stated that errors in forecasts which are used for boundary specification may play a dominant role in the evolution of limited domain forecast error. Staniforth and Mitchell (1978) tested two coarse-mesh specifications and found a more rapid decay of skill in the fine-mesh area when the coarse-mesh became less accurate.

From our results, there appears to be enough evidence to conclude that the 5° specification errors contribute up to 50% of the boundary error being generated. The rest of the error is generated from the implementation of the PK system. The errors due to boundary formulation diminish in importance when inaccurate boundary information is imposed on the limited domain forecast.

5.2. *Boundary diffusion*

Increasing the diffusion near the boundary to damp the generation of spurious waves is an important component of the PK scheme. From the evidence presented in Fig. 7, it could be argued that the lack of effective filtering may be a major factor in the generation of the formulation error of the PK scheme. The system used in the previous experiments increased the calculated diffusion five times the normal value for the first two points adjacent to the boundary and two times the normal value for the next two points. If the tendencies in the PK system are averaged after the diffusion terms are calculated (see Section 2), the actual values of diffusion turn out to be less than specified. A correcting factor was added to increase the values back to the levels used in previous PK experiments and the resulting error fields are shown in the bottom of Fig. 8. They can be compared with the unadjusted diffusion weights (top) and a moderate diffusion increase, which amounts to $\frac{2}{3}$ the values used in the final case.

The amount of diffusion used near the boundary only slightly alters the error growth. The three tests produce much smaller changes than shown for the specification experiments. Somewhat surprisingly, as the diffusion is increased, the magnitude of the errors increases. This effect may represent the increased loss in wave amplitudes entering the domain. The diffusion is increased by an order of magnitude in this case and the changes in boundary error are only 30%. In the case of the light diffusion, there still is considerable small-scale noise in the forecast (unsmoothed errors not shown). This small-scale noise is removed when the heavy diffusion is used. Increasing the diffusion near the boundary should be adjusted to minimize the growth of spurious transients, but not increased to the point of influencing the large-scale error growth. For lateral boundary formulations like the PK scheme, the problem of effectively filtering the unwanted boundary-generated transients remains unsolved.

5.3. *Boundary location*

Another character of the boundary error generation is the propagation of slow moving features inwards from the boundary. Since the interface can be considered the major source of error, a lateral shift in the boundary may significantly reduce the error in the interior. This hypothesis was tested by expanding the boundaries 20° of longitude in the west and east and moving the southern boundary northwards by 10° of latitude. The north boundary remains the same as before. This adjustment in domain checks the sensitivity of boundary changes for both active (east and west boundaries) and passive (tropical boundary) situations. It also clarifies the rate of error propagation determined previously. The resulting boundary error growth is shown in Fig. 9, which can be compared to the original errors in Fig. 3.

The boundary errors in the expanded domain along the west and east interfaces are quite different at 12 h compared to the original domain. In fact, even the sign of the error has changed indicating the strong influence of the boundary specification in determining the error. The errors at 12 h along the original domain boundary have been reduced by a factor of four. As the errors evolve during the forecast, they become more similar for both

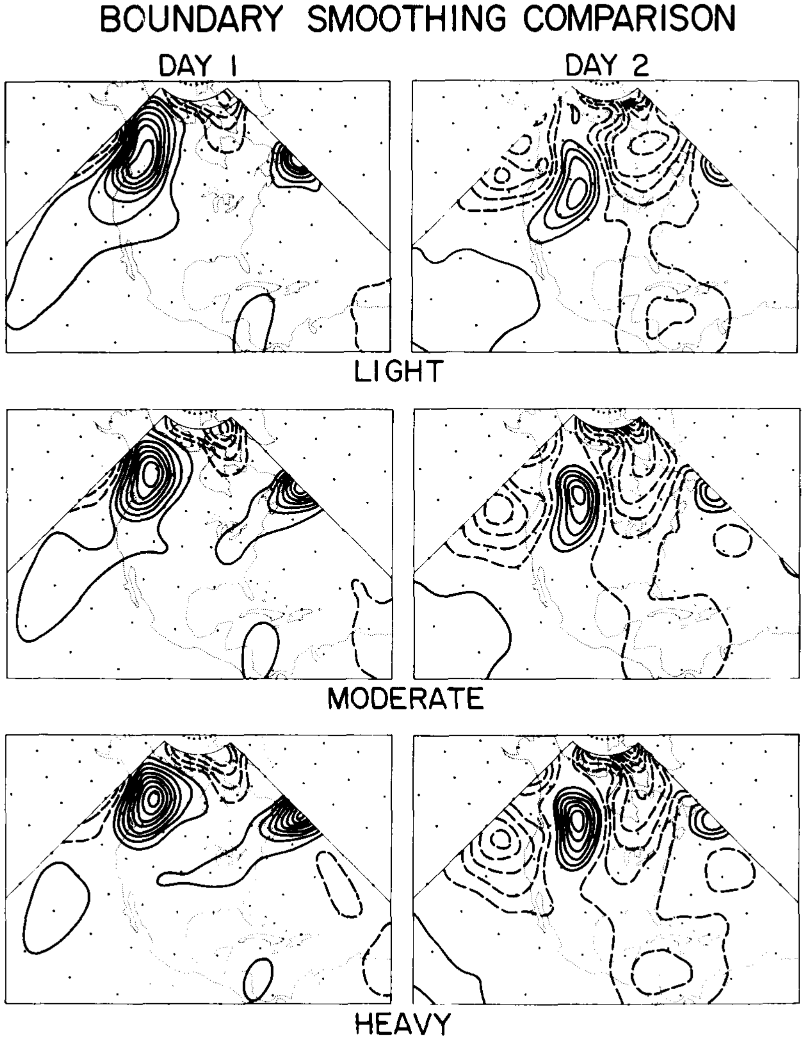

Fig. 8. Differences between bounded and unbounded 6 km pressure forecasts when light (top), moderate (middle), and heavy (bottom) applications of diffusion were added near the boundaries in the Perkey–Kreitzberg boundary condition. See text for definitions of diffusion strength. 24 h forecast (left) and 48 h forecast (right) shown. Contour interval = 1 mb with negative values dashed. Initial conditions from December 10, 1967, 1200 GMT.

domains, although the central area remains uncontaminated for a longer period in the expanded case. The propagation rates of the largest errors in the expanded case are nearly the same (30°/day) as the original domain case. Little difference in error structure is noted in the tropical region, both along the bottom and the lower sides of the new domain. By the end of the forecast, the interior errors of the expanded case have reached similar values compared to the original case. Much of this error appears to propagate from the north boundary which remained fixed.

These experiments lead to a not too surprising conclusion that boundary locations should be determined from the forecast time frame selected and the typical boundary error propagation rate. Expanding the boundaries away from areas of synoptic activity delays the growth of serious error by a rate proportional to the distance of the boundary to the area of interest. Therefore it is

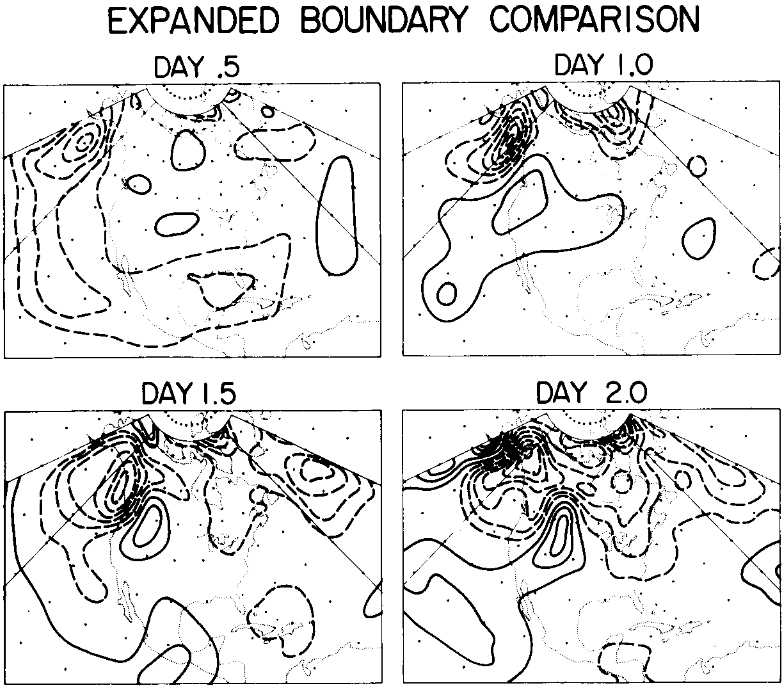

Fig. 9. Differences between bounded and unbounded 6 km pressure forecasts at 12 h (top left), 24 h (top right), 36 h (bottom left), 48 h (bottom right) for expanded domain. Domain expanded 20° of longitude in E–W direction and contracted 10° on south boundary. North boundary held fixed. Contour interval = 1 mb, negative values dashed. Initial conditions from December 10, 1967, 1200 GMT.

more important to move the synoptically active boundaries away from the area of interest than to alter inactive boundaries. For our particular selection of a 48 h forecast over the eastern U.S., the boundaries should be expanded by 20–30° from the domain shown in Fig. 3 and enlarged to the pole.

6. Comparison with Williamson–Browning method

The design of the WB system follows closely the scheme which Shapiro and O'Brien (1970) applied to the barotropic vorticity equation. The boundary values are calculated one of two ways depending on the direction of the component of the specified wind normal to the boundary. If the wind is directed into the limited-area domain, the prognostic variables are calculated from the time-space interpolated variables provided at the boundary. If the winds are directed out of the limited-area domain, the prognostic variables are extrapolated from the interior limited-area values. This extrapolation is accomplished by a time-space Lagrangian extrapolation method. The diffusion coefficient used in the deformation-type diffusion scheme (Washington and Kasahara, 1970) is increased along the boundary to hinder the reflections from returning to the interior domain.

There are three basic differences between the WB and PK schemes which deserve mentioning. First note that the PK system is applied to the variable's tendency not to the variable itself as is the case with the WB method. Second, the PK system operates over a 4Δ wide band around the boundary while the WB scheme operates only on the boundary grid points. These two differences make the PK method less likely to become unstable when a discontinuity develops between the large-scale forecast and the limited-area forecast; however, it does not necessarily ensure a minimization of spurious wave generation. The third difference concerns the inflow–outflow differentiation; PK makes no distinction between inflow and outflow boundaries while WB use a different boundary specification depending upon boundary inflow or outflow.

The implementation of the WB scheme to the Limited Area Model used in this paper is identical to that described by Williamson and Browning (1974). For the boundary error comparison, the same initial data and boundary specifications were used as in the PK experiments. Figs. 10–11 show the evolution of error produced by the WB method for the two cases. These errors should be compared to Figs. 3–4 which contain the PK error.

For the December 10 case, there is some similarity in phase and sign of the error between the two methods along the west boundary which may be traced out to 48 h; the propagation rate of this error inwards from the boundary is nearly the same in both schemes. The error amplitude is much larger for these features using the PK method. A large-scale positive error bias begins to grow in the WB method especially in the southern part of the domain. The bias grows more rapidly during the last 12 h of the forecast and begins to dominate the error structure. This problem was also present to a lesser extent in the boundary condition tests of WB (Williamson and Browning, 1974) using simulated atmospheric data.

The WB boundary condition produces much less error in the first 24 h of the forecast. The initial shocking phenomena prevalent in the PK experiment appears to be much less apparent when the WB scheme is used. After 24 h of forecasting, the error growth produced by the WB method accelerates rapidly reflecting the bias problem. In contrast, the rate of error growth has stabilized during the latter part of the forecast when the PK boundary conditions are used. In the December 14 case (Fig. 11), a similarity in error structure produced by the two methods along the west boundary for the first 24 h is again noted. There are, however, several major differences in error behavior. The early time-period advantage in error reduction produced by the WB method in the first case has been lost; both methods produce comparable errors at 12–24 h. The bias generated by the WB system also takes a different form. A very strong negative bias forms in the northern part of the domain at 36–48 h with evidence of the positive bias, found in the December 10 case, in the southern part. The contamination of boundary error in the central part of this domain also occurs more rapidly with this case. The serious errors reached the center at 30 h for the WB method and 42 h for the PK method. The error statistics derived from the WB boundary condition experiments are shown in Table 2. Many of the previously discussed results are illustrated by the statistics. The propagation effect is more clearly shown when the subset numbers are compared to the total domain values than in the PK statistics (Table 1). The WB scheme statistics for the December 10 case are superior early in the forecasts compared to PK errors. The large growth in mean error is quite apparent when the WB method is used. For the limited data sample shown here the WB boundary conditions seem more sensitive to variations in initial data than the PK scheme.

A comparison of these error statistics with other evaluations of boundary condition errors points out the similarity in behavior among many different systems and initial conditions. Earlier testing of the WB method using similar model configurations and with simulated atmospheric data derived from a GCM showed doubling of the rms error to be on the order of one day (Williamson and Browning, 1974). Experiments shown here verify these results using real atmospheric data. Miyakoda and Rosati (1977) calculated an RMS error of temperature for various boundary conditions and also found a doubling time of the order of a day. Some experiments with a finite element model (Staniforth and Mitchell, 1978) using a configuration similar to ours, half the resolution outside the boundary, and an abrupt change in gridding at the boundary again produced doubling times of about one day. Except for the early forecast oscillations in the PK errors, the doubling times for this system are also similar to the other schemes.

Forecasts made with higher computational resolution in the limited domain and the 5° boundary specification revealed a problem with the WB method. For the December 10 case and 1.25° resolution, the model integration became unstable after 36 h of forecast and similar problems developed using the December 14 data also. Increasing the diffusion near the boundary did not appreciably damp the instability. Diagnosis of the problem indicated a strong small-scale wave rapidly amplified near points with differing values of inflow/outflow immediately adjacent to and specified at the boundary. The PK boundary condition was used to make 48 h forecasts at 1.25° and .625° resolution for both sets of initial

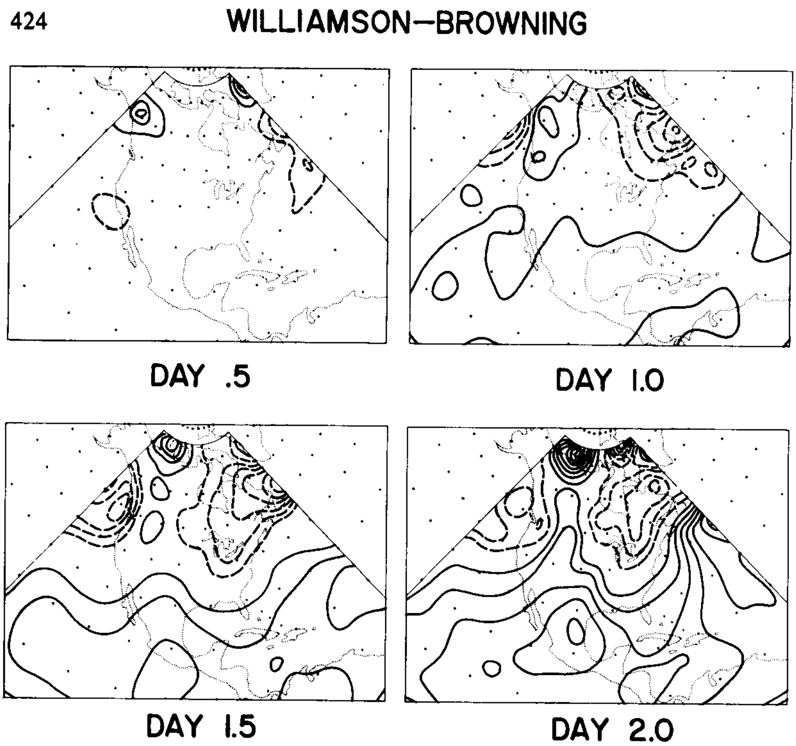

Fig. 10. Difference between bounded and unbounded 6 km pressure forecasts at 12 h (top left); 24 h (top right); 36 h (bottom left); 48 h (bottom right) using December 10, 1967, 1200 GMT initial conditions and the Williamson–Browning boundary condition. Contour interval = 1 mb. Negative values are dashed.

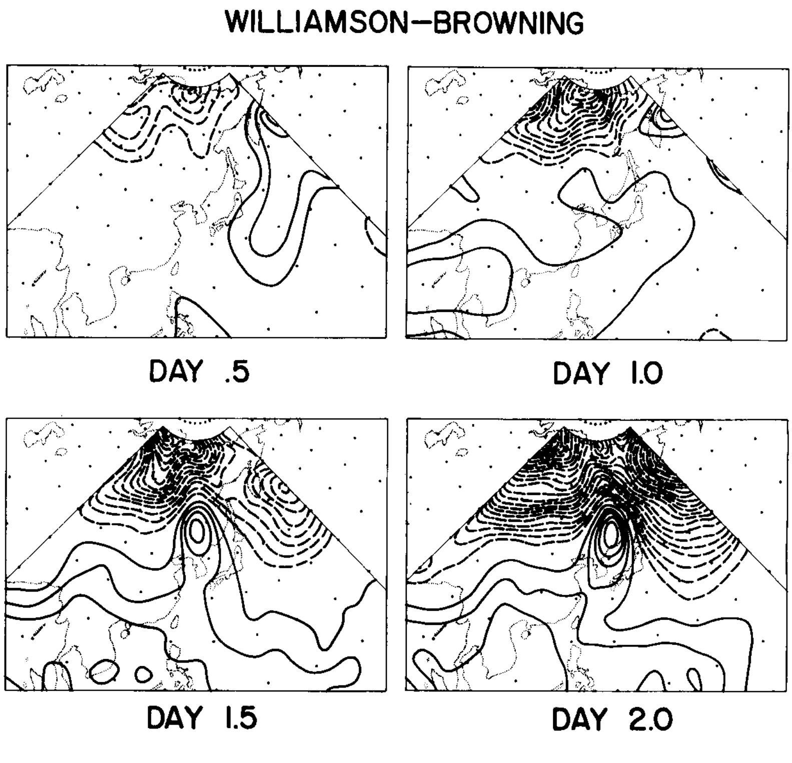

Table 2. *500 mb geopotential root mean square error (RMS), standard deviation, mean and S1 scores of the error field for the total area of the grid and a subset area (points within 20% of boundary excluded). Errors derived from WB scheme. RMS, std dev., and mean values in meters. S1 values are non-dimensional*

	Total area (subset area)			
Time	RMS	Std dev.	Mean	S1
December 10, 1967, 1200 GMT				
12H	10.3 (7.8)	10.3 (7.8)	−.8 (−.8)	15.5 (6.4)
24H	22.6 (15.4)	20.6 (12.6)	9.3 (8.8)	19.0 (7.7)
36H	34.4 (24.2)	32.4 (24.0)	11.4 (3.4)	24.9 (14.2)
48H	47.6 (38.4)	38.2 (32.8)	28.3 (20.1)	30.7 (19.1)
December 14, 1967, 1200 GMT				
12H	20.0 (13.8)	20.0 (13.6)	.2 (2.7)	17.2 (8.5)
24H	38.2 (18.7)	38.2 (15.3)	−2.1 (10.8)	26.6 (10.8)
36H	61.0 (33.2)	60.7 (31.2)	−4.6 (11.6)	31.8 (18.7)
48H	111.2 (48.7)	104.4 (48.7)	−38.2 (−11.9)	43.4 (29.9)

conditions without difficulty. Many other cases have been integrated successfully using the PK system using various configurations.

7. Relation to forecast error

In order to judge the relative significance of lateral boundary error compared to other error sources, its magnitude and growth rate are contrasted with the total forecast error (forecast minus observed). The distribution of these errors for the 24 and 48 h forecasts from the December 10, 1967 case are shown in Fig. 12. The top panel illustrates the actual forecast error for the unbounded (hemispheric) 2.5° forecast, which was used as "truth" for the boundary error calculation. The middle panel contains the limited domain forecast error using the PK scheme using the 5° boundary specification and the bottom is a reproduction of the boundary error from Fig. 3 with new contour intervals to match the top panels. For this case, the 5° unbounded forecast was nearly as accurate as the 2.5 forecast, which is somewhat unique.

Comparison of the two total error fields yields little overall difference. The basic forecast error structure is maintained when the differences can become significant. For example, the total error over the Pacific Northwest is increased by nearly 50% at 24 h (by the addition of boundary error). The total error growth rate in this case is over twice the rate in which the boundary errors are growing.

For the December 10 case, the unbounded 2.5° forecast RMS error reaches a value of 90 m at 48 h in the 20° subset area. The limited domain value is nearly the same, whereas the RMS error due to lateral boundary conditions is only one third of the total value. This case represents a rapid deterioration in forecast skill in which the specified lateral boundaries do not influence the outcome to a great extent. In the December 14 case (not shown) the total RMS error accumulation is about half the value of the first case, resulting in a more significant contribution of the boundary error to the total value. The limited area forecast RMS is about 20% worse for the total area. In this case, the boundary error is a substantial fraction of the total error field and should be remembered in subsequent interpretations.

The effect of boundary error on total forecast error appears to be case dependent and based on two factors: the location and activity on the

Fig. 11. Difference between bounded and unbounded 6 km pressure forecasts at 12 h (top left); 24 h (top right); 36 h (bottom left); 48 h (bottom right) using December 14, 1967, 1200 GMT initial conditions and the Williamson–Browning boundary condition. Contour interval = 1 mb. Negative values are dashed.

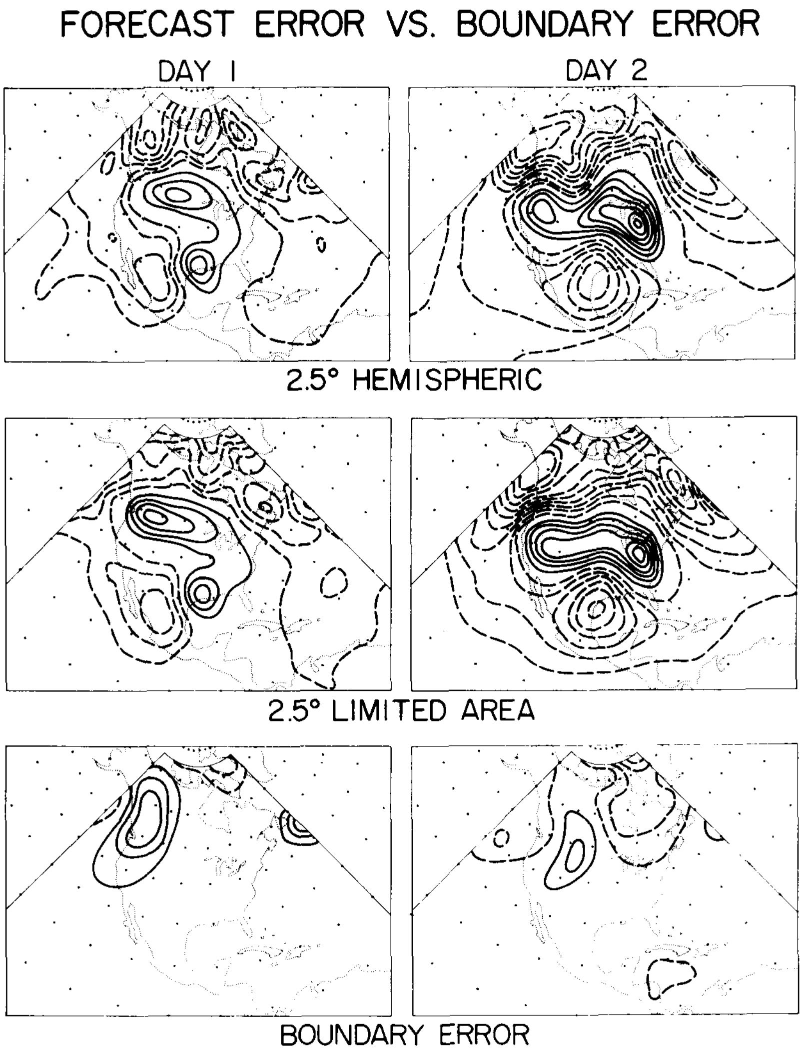

Fig. 12. 6 km pressure forecast error (forecast minus observed) for unbounded model (top), limited domain model (middle), and differences between bounded and unbounded forecasts (bottom). 24 h (left) and 48 h errors and differences (right) shown. Contour interval = 2 mb with negative values dashed. Initial conditions from December 10, 1967, 1200 GMT.

boundary and the relative accuracy of the forecast of the interior. Although there appears to be little advantage in forecasting with a finer resolution in this limited sample, experience (with other cases) has shown that this is the exception rather than the rule. Based on these results we believe limited domain models can be used to study other sources of forecast error without fear of total contamination of the results by boundary error.

8. Conclusions

The use of limited domain numerical forecast models requires the careful handling of the lateral boundaries to minimize error generation. The performance of the Perkey–Kreitzberg boundary condition was evaluated in terms of the generation of boundary error for two initial states.

The PK system proved to be a stable boundary condition for all resolutions and boundary specifications tested. The error growth rates were more rapid early in the forecast but stabilized by 24–36 h. The early error growth is related to the excitation of spurious transients which are slowly damped as the forecast progresses.

The largest errors generated by the PK system propagated inward from the boundaries at speeds of 20–30° of longitude per day. The origins of these errors were associated with large amplitude changes in the boundary specification.

Investigations into the sources of error produced by the PK method revealed several interesting facts. The specifications of the boundary values by a coarser mesh forecast can account for up to 50% of the error generation. Clearly, unless the exterior forecast is reasonably accurate, the specification error will overwhelm errors originating from the formulation of the boundary condition. The extra diffusion applied near the boundary can become a significant source of error if the amount applied becomes excessive. A balance between damping the spurious small scales and minimizing the effect of larger scales should be maintained. Expanding the active boundaries of the domain decreased the rate of contamination in the central areas. Depending on the scale of the phenomena and the time frame of interest, it is possible to determine the locations of the active boundaries to minimize error contamination in the area of interest.

A comparison with the Williamson–Browning boundary condition revealed many common error characteristics. These include the propagation of error from the boundary, sensitivity to the boundary specification, and comparable error growth doubling times in the 12–36 h range. The value of doubling is about the order of a day which agrees with other methods tested elsewhere. The WB method produced less shocking than the PK system and therefore somewhat less error early in the forecasts. The WB scheme produced low error levels only if the specified boundary values were similar to the interior forecast. When this condition was not met, rapid error growth resulted. In the case of very fine resolution forecasts specified by coarse-mesh boundary values, the error growth became unstable.

In general, the boundary errors produced by the PK scheme are much less than the total forecast error, especially if the synoptic conditions are difficult to forecast. The boundary error can be significant if the synoptic situation is easy to forecast and an unbounded forecast would produce accurate results. The general approach to lateral boundary condition formulation discussed here has been used in an operational environment at the U.S. National Weather Service with a high degree of success during the past several years. The location of the boundaries far from the area of interest has apparently been the key to their acceptable performance. The boundary conditions discussed in this paper can be successfully applied to a large number of research applications which call for limited domain integrations.

9. Acknowledgements

We would like to thank P. Downey for handling the operational aspects of these experiments. Helpful reviews of the manuscript were provided by A. Kasahara, R. Daley, T. Schlatter, T. Bettge, and J. Tribbia. The paper was typed by J. Raese, and the illustrations were drafted by J. Meehl.

REFERENCES

Anthes, R. A. 1974. Data assimilation and initialization of hurricane prediction models. *J. Atmos. Sci. 31*, 702–719.

Asselin, R. 1972. Integration of a semi-implicit model with time-dependent boundary conditions. *Atmosphere 10*, 44–55.

Baumhefner, D. P., Jenne, R. L. and Schlatter, T. W. 1978. Specialized Data Sets Available at the Nat. Center for Atmos. Res. (NCAR), WGNE Report 15, 1–3.

Charney, J. G., Fjortoft, R. and von Neumann, J. 1950. Numerical integration of the barotropic vorticity equation. *Tellus 2*, 237–254.

Davies, H. C. 1976. A lateral boundary formulation for multi-level prediction models. *Quart. J. Roy. Meteorol. Soc. 102*, 405–418.

Gauntlett, D. J., Leslie, L. M., McGregor, J. L. and Hincksman, D. R. 1978. A limited area nested numerical weather prediction model: Formulation and preliminary results. *Quart. J. Roy. Meteorol. Soc. 104*, 103–117.

Gerrity, J. F. 1977. The LFM model—1976: A documentation. *NOAA Tech. Memo. NWS NMC 60*, National Meteorological Center, NWS/NOAA, Washington, DC, p. 68.

Harrison, E. J. and Elsberry, R. L. 1972. A method for incorporating nested finite grids in the solution of systems of geophysical equations. *J. Atmos. Sci. 29*, 1235–1245.

Hodur, R. M. and Burk, S. D. 1978. The fleet numerical weather central tropical cyclone model: Comparison of cyclic and one-way interactive boundary conditions. *Mon. Wea. Rev. 106*, 1665–1671.

Hovermale, J. B., Marks, D. G. and Scolnik, S. H. 1977. Operational analysis and prediction with a movable fine-mesh system at the National Meteorological Center. *Proc.* 7th Technical Exchange Conference, El Paso, Atmos. Science Lab, White Sands, NM.

Kållberg, P. W. and Gibson, J. K. 1977. Multi-level limited area forecast using boundary zone relaxation. *WGNE Rep.* #15, p. 48.

Kesel, P. G. and Winninghoff, F. J. 1972. The Fleet Numerical Weather Central operational primitive equation model. *Mon. Wea. Rev. 100*, 360–373.

McGregor, J. L., Leslie, L. M. and Gauntlett, D. J. 1978. The ANMRC limited area model: Consolidated formulation and operational results. *Mon. Wea. Rev. 106*, 427–438.

Miyakoda, K. and Rosati, A. 1977. One-way nested grid models: The interface conditions and the numerical accuracy. *Mon. Wea. Rev. 105*, 1092–1107.

Newell, J. E. and Deaven, D. G. 1981. The LFM-II Model-1980, *NOAA Tech. Memorandum NWS NMC 66*, Nat. Meteor. Center NWS/NOAA, Washington, D.C., p. 20.

Oliger, J. and Sundström, A. 1976. Theoretical and practical aspects of some initial-boundary value problems in fluid dynamics. *STAN-CS-76-578*, Computer Science Department, Stanford University, Stanford, CA.

Perkey, D. J. 1976. A description and preliminary results from a fine-mesh model for forecasting quantitative precipitation. *Mon. Wea. Rev. 104*, 1513–1526.

Perkey, D. J. and Kreitzberg, C. W. 1976. A time-dependent lateral boundary scheme for limited-area primitive equation models. *Mon. Wea. Rev. 104*, 744–755.

Phillips, N. and Shukla, J. 1973. On the strategy of combining coarse and fine grid meshes in numerical weather prediction. *J. Appl. Meteorol. 12*, 763–770.

Phillips, N. 1978. The nested grid model. *NOAA Tech. Reports*, NWS, 96.

Shapiro, M. A. and O'Brien, J. J. 1970. Boundary conditions for fine-mesh limited-area forecasts. *J. Appl. Meteorol. 9*, 345–349.

Staniforth, A. N. and Mitchell, H. L. 1978. A variable-resolution finite-element technique for regional forecasting with the primitive equations. *Mon. Wea. Rev. 106*, 439–447.

Sundström, A. and Elvius, T. 1979. Numerical Methods Used in Atmospheric Models—Vol. II, Chap. 7 (Computational Problems Related to Limited area Modeling). GARP publication series #17, WMO, p. 495.

Teweles, S. and Wobus, H. B. 1954. Verification of Prognostic Charts. *Bull. Am. Meteorol. Soc. 35*, 455–463.

Valent, R. A., Downey, P. H. and Donnelly, J. L. 1977. Description and operational aspects of the NCAR Segmented Limited Area Model (LAMSEG), NCAR Report #0501-77/08, 105.

Washington, W. M. and Kasahara, A. 1970. A January simulation experiment with the two-layer version of the NCAR global circulation model. *Mon. Wea. Rev. 98*, 559–580.

Washington, W. M. and Baumhefner, D. P. 1975. A method of removing lamb waves from initial data for primitive equation models. *J. Appl. Meteorol. 14*, 114–119.

Washington, W. M., Otto-Bliesner, B. and Williamson, G. 1977. January and July simulation experiments with the 2.5° latitude–longitude version of the NCAR General Circulation Model. *NCAR Tech. Note #123 + STR*, p. 39.

Williamson, D. L. 1976. Normal mode initialization procedure applied to forecasts with the global shallow water equations. *Mon. Wea. Rev. 104*, 195–206.

Williamson, D. L. and Browning, G. L. 1974. Formulation of the lateral boundary conditions for the NCAR limited area model. *J. Appl. Meteorol. 13*, 8–15.